# Letters

## A Virtual *RLC* Damper to Stabilize DC/DC Converters Having an *LC* Input Filter while Improving the Filter Performance

Xin Zhang, *Member, IEEE*, Qing-Chang Zhong, *Senior Member, IEEE*, and Wen-Long Ming

***Abstract*—The $LC$ filter at the input of a dc/dc converter may cause instability when the converter is controlled as a constant power load (CPL) and one of the effective solutions is to reduce the output impedance of the $LC$ input filter with different stabilization dampers. In this letter, the impact of these dampers on the $LC$ filter is analyzed with two-port network analysis and it is found that the existing dampers all degrade the performance of the original $LC$ input filter to some extent. In order to overcome this drawback, an $RLC$ damper is proposed to stabilize the whole system while improving the performance of the $LC$ input filter. In addition, this $RLC$ damper is also designed to achieve high robustness against the parameter variations of the $LC$ input filter. Furthermore, in order to avoid the power loss when implementing the damper physically, a control strategy for the CPL is proposed to implement the $RLC$ damper as a virtual $RLC$ ($VRLC$) damper. The actual effectiveness of the $VRLC$ damper and its impact on the CPL are fully evaluated via two-port network analysis as well. Finally, experimental results from a 100-W 48–24-V buck converter with an $LC$ input filter are presented to demonstrate the proposed $VRLC$ damper.**

***Index Terms*—Constant power load, dynamic, input filter, robustness, stability, two-port network, virtual *RLC* damper.**

### I. Introduction

MOST dc/dc converters in practice are cascaded with an $LC$ input filter to mitigate the propagation of switching harmonics back into the source [1]. However, the tightly regulated dc/dc converters always behave as constant power load (CPL) and have a negative incremental input resistance within the bandwidth of its control loop, which reduces the system damping and may destabilize the system [2], [3].

Since the reduced system damping caused by the CPL is the root of instability problem in cascaded systems [2], the most intuitive solution is to increase the system damping by using dampers [4]–[6]. Three typical dampers are depicted in Fig. 1, where the elements in the dashed line are used for damping. They are called the $RC$ parallel damper [see Fig. 1(a)], the $RL$ parallel damper [see Fig. 1(b)] and the $RL$ series damper [see Fig. 1(c)], respectively. For the system shown in Fig. 1(d) with these dampers, the peak of the output impedance of the $LC$ input filter can be damped and a total separation between $|Z_o|$ and $|Z_{iL}|$ can be ensured to fulfil Middlebrook criterion [2]. Here, $Z_o$ is the output impedance of the damped $LC$ input filter and $Z_{iL}$ is the input impedance of the CPL.

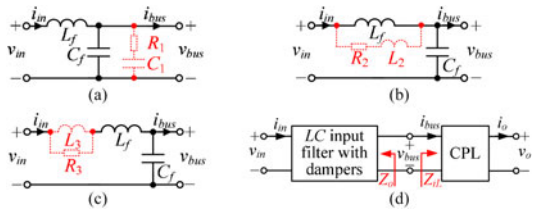


Fig. 1. Typical dampers and application. (a) $RC$ parallel damper. (b) $RL$ parallel damper. (c) $RL$ series damper. (d) Application.

Although these filter dampers can stabilize the cascaded system, their impact on the $LC$ input filter is always ignored and rarely reported. In this letter, their impact is carefully analyzed via two-port network analysis and it is found that, all these dampers degrade the original $LC$ input filter performance to some extent. To solve this problem, an $RLC$ damper is proposed in this letter, which not only can stabilize the system with improving the performance of the $LC$ input filter, but also can achieve high robustness to the parameter variations of the $LC$ input filter. By the $RLC$ damper, a virtual $RLC$ ($VRLC$) damper is further proposed to avoid the power loss of the passive components via changing the control block of the CPL. It should be stressed that, though the $VRLC$ damper is similar with the PVI control strategy in [7], they are essentially different. The PVI control strategy stabilizes the system via shaping the load input impedance without considering the source performance. However, the $VRLC$ damper stabilizes the system by shaping the output impedance of the $LC$ input filter while improving the filter performance. Finally, the proposed $VRLC$ damper is experimentally verified by a 100-W buck converter with an $LC$ input filter.

### II. Existing Dampers and Their Impact on the $LC$ Input Filter

#### A. Review of the Existing Dampers

In this section, the existing dampers are reviewed under the same design principle: 6-dBΩ system gain margin (GM) [8].

*1) RC Parallel Damper:* According to [4], Fig. 1(a) and 6-dBΩ GM stability requirement, the components $C_1$ and $R_1$ of

Manuscript received February 19, 2016; revised March 19, 2016; accepted April 08, 2016. Date of publication April 13, 2016; date of current version July 08, 2016. This work was supported by the Engineering and Physical Sciences Research Council, U.K., under Grant EP/I038586/1.

X. Zhang and W.-L. Ming are with the Department of Automatic Control and Systems Engineering, The University of Sheffield, Sheffield S1 3JD, U.K. (e-mail: xin.zhang@sheffield.ac.uk; wenlongming@gmail.com).

Q.-C. Zhong is with the Department of Electrical and Computer Engineering, Illinois Institute of Technology, Chicago, IL 60616 USA, and also with the Department of Automatic Control and Systems Engineering, The University of Sheffield, Sheffield S1 3JD, U.K. (e-mail: zhongqc@ieee.org).

Color versions of one or more of the figures in this paper are available online at http://ieeexplore.ieee.org.

Digital Object Identifier 10.1109/TPEL.2016.2553786

the $RC$ parallel damper can be designed as

$$C_1 = n_1 C_f \tag{1}$$

$$R_1 = R_{\rm of}\sqrt{(2+n_1)(4+3n_1)\Big/[2n_1^2(4+n_1)]} \tag{2}$$

where

$$R_{\rm of} = \sqrt{L_f/C_f}, n_1 = \left[R_{\rm of}^2\Big/\left(Z_{iL}/10^{\frac{6}{20}}\right)^2\right] \cdot\left\{1+\sqrt{1+4\left[\left(Z_{iL}/10^{\frac{6}{20}}\right)^2\Big/R_{\rm of}^2\right]}\right\}.$$

*2) RL Parallel Damper:* According to [4], Fig. 1(b) and 6-dBΩ GM stability requirement, the components $L_2$ and $R_2$ of the $RL$ parallel damper can be designed as

$$L_2 = n_2 L_f \tag{3}$$

$$R_2 = R_{\rm of}\sqrt{n_2(3+4n_2)(1+2n_2)\Big/[2(1+4n_2)]} \tag{4}$$

where $n_2 = \frac{1}{4}\{\sqrt{1+4[(Z_{iL}/10^{\frac{6}{20}})^2/R_{\rm of}^2]}-1\}$.

*3) RL Series Damper:* According to [4], Fig. 1(c) and 6-dBΩ GM stability requirement, the components $L_3$ and $R_3$ of the $RL$ series damper can be designed as

$$L_3 = n_3 L_f \tag{5}$$

$$R_3 = R_{\rm of}\left[\frac{(1+n_3)}{n_3}\sqrt{\frac{2(1+n_3)(4+n_3)}{(2+n_3)(4+3n_3)}}\right]^{-1} \tag{6}$$

where

$$n_3 = \left[\sqrt{1+4\left[\left(Z_{iL}\Big/10^{\frac{6}{20}}\right)^2\Big/R_{\rm of}^2\right]}+3\right] \cdot\left\{\left[\left(Z_{iL}\Big/10^{\frac{6}{20}}\right)^2\Big/R_{\rm of}^2\right]-2\right\}^{-1}.$$

It is known that, all the aforementioned dampers can ensure a total separation between $|Z_o|$ and $|Z_{iL}|$ to stabilize the system [4], [5]. However, their impact on the $LC$ input filter has not been analyzed enough in the existing literature. Therefore, the impact of existing dampers on the $LC$ input filter is carefully analyzed by two-port network model in Section II-B and II-C.

### *B. Generic Two-Port Network Model of the LC Input Filter With Different Dampers*

In Fig. 2(a), the generic two-port network circuit model of the $LC$ input filter with different dampers is presented, where $v_{\rm in}$ and $v_{\rm bus}$ are the filter input and output voltage, respectively; $i_{\rm in}$ and $i_{\rm bus}$ are the filter input and output current, respectively; $A_x(s)$ and $B_x(s)$ represents the impedance of the filter inductor branch and capacitor branch, respectively. The further description of $A_x(s)$ and $B_x(s)$ is presented in Table I. In Fig. 2(b), the two-port block diagram of Fig. 2(a) is given, where $Z_{\rm ox}(s)$

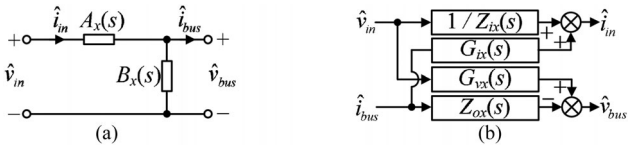


Fig. 2. Generic two-port network model of the $LC$ input filter with different dampers. (a) Circuit model. (b) Block diagram.

TABLE I
DEFINITIONS OF $A_x(s)$ AND $B_x(s)$ IN DIFFERENT DAMPERS

| *LC* input filter | $A_x$ | $B_x$ |
|---|---|---|
| Original (*x*=0) | $L_f$ | $C_f$ |
| *RC* parallel damper (*x*=1) | $L_f$ | $R_1$ $C_f$ $C_1$ |
| *RL* parallel damper (x=2) | $L_f$ $R_2$ $L_2$ | $C_f$ |
| *RL* series damper (x=3) | $L_3$ $R_3$ $L_f$ | $C_f$ |
| Proposed damper (x=4) | $L_f$ | $C_f$ $R_4$ $L_4$ $C_4$ |

is the output impedance; $1/Z_{\rm ix}(s)$ is the input voltage to input current transfer function; $G_{\rm vx}(s)$ is the input to output voltage transfer function; and $G_{\rm ix}(s)$ is the load to input current transfer function. Here, the subscript $x = 0 \sim 4$ denote the cases with no damper, $RC$ parallel damper, $RL$ parallel damper, $RL$ series damper, and the latter proposed damper, respectively. As well known, the performance of the $LC$ input filter can be fully described by $Z_{\rm ox}(s) \sim G_{\rm ix}(s)$, which can be derived as

$$Z_{\rm ox}(s) = -\frac{\hat{v}_{\rm bus}(s)}{\hat{i}_{\rm bus}(s)}\bigg|_{\hat{v}_{\rm in}(s)=0} = \frac{A_x(s)\cdot B_x(s)}{A_x(s)+B_x(s)} \tag{7}$$

$$1/Z_{\rm ix}(s) = \frac{\hat{i}_{\rm in}(s)}{\hat{v}_{\rm in}(s)}\bigg|_{\hat{i}_{\rm bus}(s)=0} = \frac{1}{A_x(s)+B_x(s)} \tag{8}$$

$$G_{\rm vx}(s) = \frac{\hat{v}_{\rm bus}(s)}{\hat{v}_{\rm in}(s)}\bigg|_{\hat{i}_{\rm bus}(s)=0} = \frac{B_x(s)}{A_x(s)+B_x(s)} \tag{9}$$

$$G_{\rm ix}(s) = \frac{\hat{i}_{\rm in}(s)}{\hat{i}_{\rm bus}(s)}\bigg|_{\hat{v}_{\rm in}(s)=0} = \frac{B_x(s)}{A_x(s)+B_x(s)}. \tag{10}$$

### *C. Impact of Existing Dampers on the LC Input Filter via Two-port Network Analysis*

According to Section II-B, the performance of the $LC$ input filter can be fully evaluated by two-port network analysis with four transfer functions: $Z_{\rm ox}(s)$, $1/Z_{\rm ix}(s)$, $G_{\rm vx}(s)$, and $G_{\rm ix}(s)$, where $Z_{\rm ox}(s)$ reflects the impact of the (load) current $i_{\rm bus}$ on the (load) voltage $v_{\rm bus}$; $1/Z_{\rm ix}(s)$ reflects the impact of (input) voltage variations of $v_{\rm in}$ on the (input) current $i_{\rm in}$; $G_{\rm vx}(s)$ reflects the impact of (input) voltage variations of $v_{\rm in}$ on the (load) voltage $v_{\rm bus}$; and $G_{\rm ix}(s)$ reflects the impact of the (load) current $i_{\rm bus}$ on the (input) current $i_{\rm in}$. However, all the existing dampers are only focused on how to damp $|Z_{\rm ox}(s)|$ to ensure the system stability while ignoring their other impact on $Z_{\rm ox}(s)$, $1/Z_{\rm ix}(s)$, $G_{\rm ix}(s)$, and $G_{\rm vx}(s)$. Therefore, in order to analyze the impact of the existing dampers on the $LC$ input filter, the existing dampers impact on $Z_{\rm ox}(s)$, $1/Z_{\rm ix}(s)$, $G_{\rm vx}(s)$, and $G_{\rm ix}(s)$ are thoroughly analyzed in this section. Moreover, in order to show the results in a clear way, a specific $LC$ input filter is taken as an example to facilitate the analysis. The parameters of the example $LC$ input

TABLE II
PARAMETERS OF THE EXAMPLE $LC$ INPUT FILTER WITH DIFFERENT DAMPERS

| PARM | Value | PARM | Value | PARM | Value | PARM | Value |
|---|---|---|---|---|---|---|---|
| $V_{\text{in}}$ | 48 V | $C_f$ | 50 $\mu$F | $L_2$ | 1.5 mH | $L_4$ | 1.9 mH |
| $V_{\text{bus}}$ | 48 V | $R_1$ | 6.5 $\Omega$ | $R_3$ | 1.7 $\Omega$ | $C_4$ | 27 $\mu$F |
| $P_0$ | 100 W | $C_1$ | 60 $\mu$F | $L_3$ | 1 mH | | |
| $L_f$ | 1 mH | $R_2$ | 6.5 $\Omega$ | $R_4$ | 11.5 $\Omega$ | | |

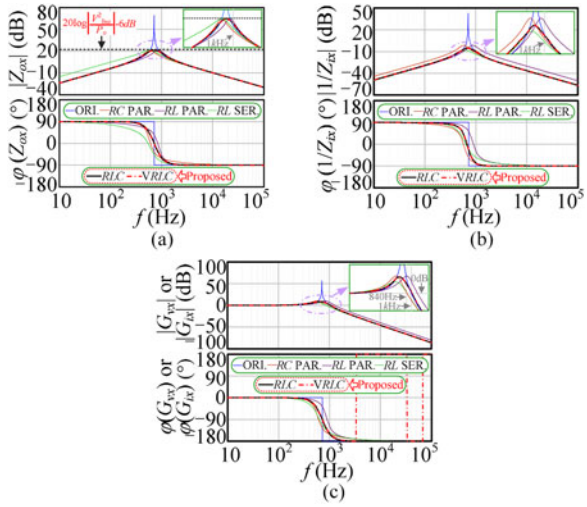


Fig. 3. Impact of different dampers on the $LC$ input filter. (a) $Z_{\text{ox}}(s)$; (b) $1/Z_{\text{ix}}(s)$; (c) $G_{\text{vx}}(s)$; and $G_{\text{ix}}(s)$.

filter and its dampers are given in Table II, where the existing dampers are designed according to [4] with 6-dB$\Omega$ system GM. In addition, For the CPL, its $Z_{iL}$ is equal to $-V_{\text{bus}}^2/P_o$, where $P_o$ is the output power of the CPL and its value is also listed in Table II.

According to (7) and Table I and II, the Bode plots of $Z_{\text{ox}}(s)$ with different dampers are depicted in Fig. 3(a). It is shown that, the peak of $|Z_{\text{ox}}(s)|$ can be damped by all the dampers to ensure 6-dB$\Omega$ GM stability of the cascaded system. However, the $RL$ series damper increases $|Z_{\text{ox}}(s)|$ at the lower frequency range. Since a higher $|Z_{\text{ox}}(s)|$ means a poorer suppression ability of $v_{\text{bus}}$ to the disturbance of $i_{\text{bus}}$, the $RL$ series damper has worse impact on $Z_{\text{ox}}(s)$.

According to (8) and Table I and II, the Bode plots of $1/Z_{\text{ix}}(s)$ with different dampers are presented in Fig. 3(b). It is shown that, though the peak of $|1/Z_{\text{ix}}(s)|$ can be damped by all the dampers, the $RC$ parallel and $RL$ parallel dampers increase $|1/Z_{\text{ix}}(s)|$ at the lower and higher frequency range, respectively. Since a higher $|1/Z_{\text{ix}}(s)|$ means a worse suppression ability of $i_{\text{in}}$ to the disturbance of $v_{\text{in}}$, both $RC$ parallel and $RL$ parallel dampers have worse impact on $1/Z_{\text{ix}}(s)$.

By (9) and (10), since $G_{\text{vx}}(s)$ is same with $G_{\text{ix}}(s)$, they are depicted by the same Bode plots in Fig. 3(c).

For $G_{\text{vx}}(s)$, if it has a higher cutoff frequency, $v_{\text{bus}}$ will have a quick dynamic response to $v_{\text{in}}$. According to Fig. 3(c), the cutoff frequency of $G_{\text{vx}}(s)$ is increased when adopting the $RL$ parallel damper, but reduced when adopting the $RC$ parallel or $RL$ series dampers. Therefore, the $RL$ parallel damper has better impact, but the $RC$ parallel and $RL$ series dampers have worse impact on $G_{\text{vx}}(s)$.

TABLE III
IMPACT ON $LC$ INPUT FILTER WITH DIFFERENT DAMPERS

| Damper \ Impact | $Z_{ox}(s)$ | $1/Z_{ix}(s)$ | $G_{vx}(s)$ | $G_{ix}(s)$ | System stability |
|---|---|---|---|---|---|
| Without damper | Normal | Normal | Normal | Normal | Unstable |
| *RC* PAR. | Better | Worse | Worse | Better | Stable |
| *RL* PAR. | Better | Worse | Better | Worse | Stable |
| *RL* SER. | Worse | Better | Worse | Better | Stable |
| Proposed damper | Better | Better | Better | Better | Stable |

For $G_{\text{ix}}(s)$, since it reflects the suppression capability of $i_{\text{in}}$ to the harmonic of $i_{\text{bus}}$, it determines the resistance to electromagnetic interference of the $LC$ input filter [4]. Therefore, the lower cutoff frequency of $G_{\text{ix}}(s)$ and the smaller $|G_{\text{ix}}(s)|$, the better. By Fig. 3(c), the resonant peak of $|G_{\text{ix}}(s)|$ is damped by all the dampers, the cutoff frequency and amplitude of $G_{\text{ix}}(s)$ is reduced by both $RC$ parallel and $RL$ series dampers. However, the $RL$ parallel damper increases the cutoff frequency and amplitude of $G_{\text{ix}}(s)$. Hence, both $RC$ parallel and $RL$ series dampers have better impact, but $RL$ parallel damper has worse impact on $G_{\text{ix}}(s)$.

The impact of the existing dampers on the $LC$ input filter is finally concluded in Table III. Although all the existing dampers can realize their stabilization function, they degrade the performance of the $LC$ input filter to some extent. Note that, the impact of the damper to be proposed later on the $LC$ input filter is also included in Table III for comparison.

## III. PROPOSED $RLC$ DAMPER

### A. Design Principle of the Proposed $RLC$ Damper

To overcome the drawbacks of the existing dampers, an $RLC$ damper is proposed, which is added in parallel with the output of the $LC$ input filter and composed by a resistor $R_4$, an inductor $L_4$, and a capacitor $C_4$ [see Fig. 4(a)]. The impedance of this $RLC$ damper is $Z_{RLC}(s) = R_4 + sL_4 + (1/sC_4)$, whose Bode plot is depicted in Fig. 4(b). As seen, the characteristics of $Z_{RLC}(s)$ is similar with a band-stop filter, whose stop band is $(f_1,\ f_2)$: If $f < f_1$, $Z_{RLC}(s) = 1/sC_4$; If $f \in [f_1,\ f_2]$, $Z_{RLC}(s) = R_4$; and If $f > f_1$, $Z_{RLC}(s) = sL_4$. Thus, the $RLC$ damper only plays its damper function during $[f_1,\ f_2]$, in which $R_4$ is equivalently added in parallel with $Z_{o0}$. Here, $f_1 = 1/(2\pi R_4 C_4)$ and $f_2 = R_4/(2\pi L_4)$.

For the CPL and its input $LC$ filter, if their system does not have enough stability GM, $|Z_{o0}(s)|$ will be intersected with $|Z_{iL}/10^{(GM/20)}|$. Considering $Z_{o0}(s) = sL_f/(s^2L_fC_f + 1)$ and $Z_{iL}(s) = -V_{\text{bus}}^2/P_o$, the Bode plots of $Z_{o0}(s)$ and $Z_{iL}/10^{(GM/20)}$ are depicted in Fig. 4(c). As seen, $|Z_{o0}(s)|$ is intersected with $|Z_{iL}/10^{(GM/20)}|$ at $f_L$ and $f_H$, where

$$f_L = \frac{P_o 10^{\frac{GM}{20}}}{4\pi C_f V_{\text{bus}}^2}\left(\sqrt{1+\frac{4V_{\text{bus}}^4 C_f}{P_o^2 10^{\frac{GM}{10}} L_f}} - 1\right) \tag{11}$$

$$f_H = \frac{P_o 10^{\frac{GM}{20}}}{4\pi C_f V_{\text{bus}}^2}\left(\sqrt{1+\frac{4V_{\text{bus}}^4 C_f}{P_o^2 10^{\frac{GM}{10}} L_f}} + 1\right). \tag{12}$$

Since $Z_{o4}(s) = Z_{o0}(s) \parallel Z_{RLC}(s)$ and by Fig. 4(b) and (c), if the system GM is required to be realized with a minimum impact of the $RLC$ damper, three basic design principles of the $RLC$ damper should be satisfied: 1) $R_4 = |(V_{\text{bus}}^2)/[P_o 10^{(GM/20)}]|$; 2) $f_1 = f_{L\min}$; and 3) $f_2 = f_{H\max}$.

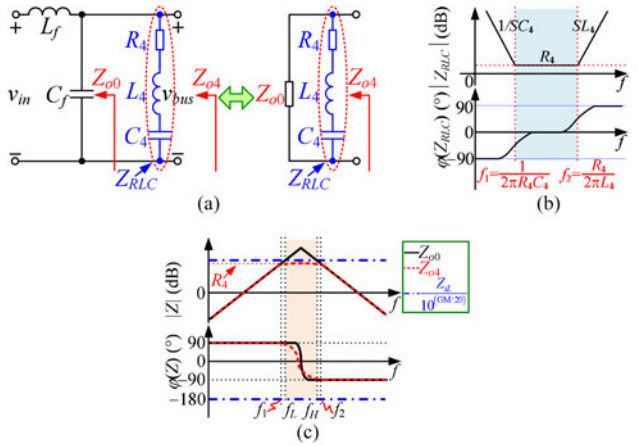


Fig. 4. Proposed $RLC$ damper. (a) Structure. (b) Characteristics. (c) Design principle.

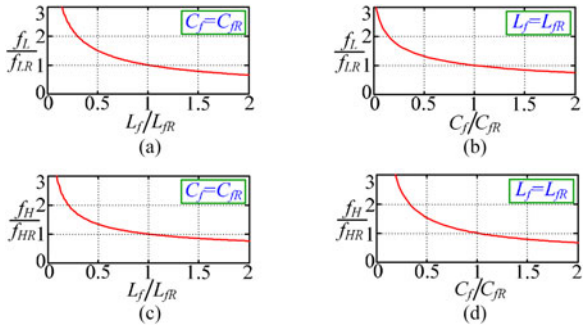


Fig. 5. Relationship between $f_L$, $f_H$ and $L_f$, $C_f$. (a) $\frac{f_L}{f_{LR}}$ versus $\frac{L_f}{L_{fR}}$. (b) $\frac{f_L}{f_{LR}}$ versus $\frac{C_f}{C_{fR}}$. (c) $\frac{f_H}{f_{HR}}$ versus $\frac{L_f}{L_{fR}}$. (d) $\frac{f_H}{f_{HR}}$ versus $\frac{C_f}{C_{fR}}$.

Here, $f_{L\min}$ is the minimum value of $f_L$, $f_{H\max}$ is the maximum value of $f_{H\max}$. Following the aforementioned design principles, the Bode plot of $Z_{o4}(s)$ is plotted with dashed lines in Fig. 4(c). As seen, $|Z_{o4}(s)|$ is only changed during $[f_1,\ f_2]$ and always lower than $|Z_{iL}/10^{(GM/20)}|$ to ensure the system GM.

### *B. Parameters Selection of the RLC Damper to Achieve High Robustness Against the Variations of $L_f$ and $C_f$*

According to Section III-A, the impedance characteristics of the $RLC$ damper behaves like a band-stop filter shown in Fig. 4(b), whose stop band is $(f_1,\ f_2)$. As discussed before, if the $RLC$ damper wants to stabilize the whole system with a minimum impact on the $LC$ input filter, $f_1$ and $f_2$ should be equal to $f_{L\min}$ and $f_{H\max}$, respectively. However, according to (11) and (12), both $f_L$ and $f_H$ are affected by $L_f$ and $C_f$. In Fig. 5(a) and (b), the curves of $\frac{f_L}{f_{LR}}$ versus $\frac{L_f}{L_{fR}}$ or $\frac{C_f}{C_{fR}}$ are presented, respectively. Here, $L_{fR}$ and $C_{fR}$ are the rated value of $L_f$ and $C_f$, respectively, $f_{LR}$ is the value of $f_L$ under $L_{fR}$ and $C_{fR}$. As seen, $f_L$ is monotonically decreased when $L_f$ or $C_f$ increases. Similarly, the curves of $\frac{f_H}{f_{HR}}$ versus $\frac{L_f}{L_{fR}}$ or $\frac{C_f}{C_{fR}}$ are also presented in Fig. 5(c) and (d), respectively, where $f_{HR}$ is the value of $f_H$ under $L_{fR}$ and $C_{fR}$. It is shown that, $f_H$ is also monotonically decreased when $L_f$ or $C_f$ increases.

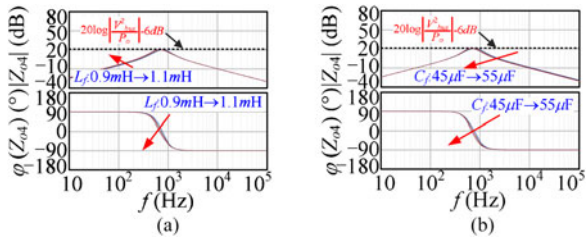


Fig. 6. Bode plots of $Z_{o4}(s)$: (a) $L_f$ : 0.9 mH $\rightarrow$ 1.1 mH, $C_f = 50\ \mu$F; (b) $L_f = 1$ mH, $C_f$ : 45 $\mu$F $\rightarrow$ 55 $\mu$F.

In practice, the value of $L_f$ and $C_f$ are not constant but varied according to different operation conditions, such as working frequency and temperature. Here, it is assumed that, the value of $L_f$ or $C_f$ is varied between $(\alpha_L L_{fR} \sim \beta_L L_{fR})$ or $(\alpha_C C_{fR} \sim \beta_C C_{fR})$, respectively, then according to Fig. 5, the expression of $f_{L\min}$ and $f_{H\max}$ can be derived as

$$f_{L\min} = \frac{P_o 10^{\frac{GM}{20}}}{4\pi C_\beta V_{\text{bus}}^2}\left(\sqrt{1+\frac{4V_{\text{bus}}^4 C_\beta}{P_o^2 10^{\frac{GM}{10}} L_\beta}}-1\right) \quad (13)$$

$$f_{H\max} = \frac{P_o 10^{\frac{GM}{20}}}{4\pi C_\alpha V_{\text{bus}}^2}\left(\sqrt{1+\frac{4V_{\text{bus}}^4 C_\alpha}{P_o^2 10^{\frac{GM}{10}} L_\alpha}}+1\right) \quad (14)$$

where $C_\beta = \beta_C C_{fR}$, $L_\beta = \beta_L L_{fR}$, $C_\alpha = \alpha_C C_{fR}$, and $L_\alpha = \alpha_L L_{fR}$.

Since $f_1 = f_{L\min}$ and $f_2 = f_{H\max}$, by Fig. 4(b), (13), and (14), the parameters of the $RLC$ damper can be selected as

$$L_4 = R_4 \Big/ \left[\frac{P_o 10^{\frac{GM}{20}}}{2C_\alpha V_{\text{bus}}^2}\left(\sqrt{1+\frac{4V_{\text{bus}}^4 C_\alpha}{P_o^2 10^{\frac{GM}{10}} \alpha_L L_\alpha}}+1\right)\right] \quad (15)$$

$$C_4 = 1 \Big/ \left[\frac{R_4 P_o 10^{\frac{GM}{20}}}{2C_\beta V_{\text{bus}}^2}\left(\sqrt{1+\frac{4V_{\text{bus}}^4 C_\beta}{P_o^2 10^{\frac{GM}{10}} L_\beta}}-1\right)\right] \quad (16)$$

where $R_4 = |V_{\text{bus}}^2/[P_o 10^{(GM/20)}]|$.

To further verify the correctness of the robust design of the $RLC$ damper, (15) and (16) are substituted into the example $LC$ input filter of Table II to calculate $R_4$, $L_4$, and $C_4$ under the following assumptions: $\alpha_L = \alpha_C = 0.9$; $\beta_L = \beta_C = 1.1$. As a result, $R_4 = 11.5\,\Omega$, $L_4 = 1.9$ mH, and $C_4 = 27\ \mu$F. By the calculated parameters, the Bode plots of $Z_{o4}(s)$ with the variations of $L_f$ or $C_f$ are depicted in Fig. 6(a) and (b), respectively. As seen, whether $L_f$ or $C_f$ varies within 0.9 $\sim$ 1.1 of its rated value, $|Z_{o4}(s)|$ is always lower than $|Z_{iL}/10^{(GM/20)}|$ $(GM = 6\text{dB})$ to realize its damping function. Therefore, the designed $RLC$ damper indeed achieves high robustness against the variations of $L_f$ and $C_f$.

### *C. Impact of the RLC Damper on the LC Input Filter*

By (7)–(10) and Table I and II, the Bode plots of $Z_{\text{ox}}(s)$, $1/Z_{\text{ix}}(s)$, $G_{\text{vx}}(s)$, and $G_{\text{ix}}(s)$ of the $LC$ input filter with the $RLC$ damper are also depicted in Fig. 3. It is shown that, compared with the existing dampers, the $RLC$ damper not only has the same stabilization function, but also has better impact on

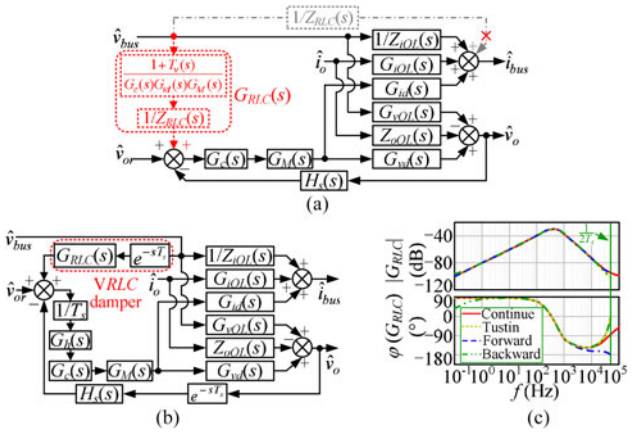


Fig. 7. Control strategy of the $VRLC$ damper. (a) Concept. (b) Digital implementation. (c) Discretization effect of $G_{RLC}(s)$.

all the transfer functions (e.g., $Z_{\rm ox}(s)$, $1/Z_{\rm ix}(s)$, $G_{\rm vx}(s)$, and $G_{\rm ix}(s)$) of the $LC$ input filter. The impact of the proposed $RLC$ damper on the $LC$ input filter is also recorded in Table III as "proposed damper." It is shown that, the proposed $RLC$ damper is better than the existing dampers.

## IV. Virtual Implementation of the Proposed $RLC$ Damper

### A. Concept and Implementation of the $VRLC$ Damper

According to Fig. 4(a), since the proposed $RLC$ damper is required to be added in parallel with output port of the $LC$ input filter, it certainly can be realized by putting a virtual $RLC$ ($VRLC$) damper in parallel with the input port of the CPL via control method to avoid additional power loss. This is the initial inspiration of the $VRLC$ damper.

As shown in Fig. 7(a), the small-signal control block of a typical CPL is presented. Its variables and transfer functions are also described in Fig. 7(a). Obviously, one intuitive way to realize the $VRLC$ damper is introducing its admittance $1/Z_{RLC}(s)$ to the control block of the CPL between its input voltage $v_{\rm bus}$ and input current $i_{\rm bus}$, as shown in the darked dot-dashed lines in Fig. 7(a). However, this method cannot be achieved by control directly, thus, the output of $1/Z_{RLC}(s)$ is moved to the output voltage reference and equivalent adjusts the transfer function to $G_{RLC}(s)$, as shown with the dashed lines in Fig. 7(a). Fig. 7(a) fully presents the concept of the $VRLC$ damper, and $G_{RLC}(s)$ can be expressed as

$$G_{RLC}(s) = \frac{1}{Z_{RLC}(s)} \frac{1+T_v(s)}{G_c(s)G_{id}(s)G_M(s)} \tag{17}$$

where $T_v(s) = H_s(s)G_c(s)G_M(s)G_{vd}(s)$ is the loop gain of the voltage closed loop of the CPL.

In practice, the $VRLC$ damper can be implemented by a digital control chip, such as a digital signal processor or a microcontroller unit. In Fig. 7(b), the digital-control-based small-signal model of the CPL with the $VRLC$ damper is presented. As seen, the digital control introduces two types of delay to the control system: the computation delay and the pulsewidth modulation (PWM) delay [9]. The computation delay is one sampling period in the commonly used synchronous sampling scheme, which can be modeled as $e^{-T_s s}$. The PWM delay is caused by the zero-order hold effect, which can be expressed as $G_h(s) = (1-e^{-T_s s})/s \approx T_s e^{-0.5T_s s}$. Here, $T_s$ is the sampling time of the digital control system.

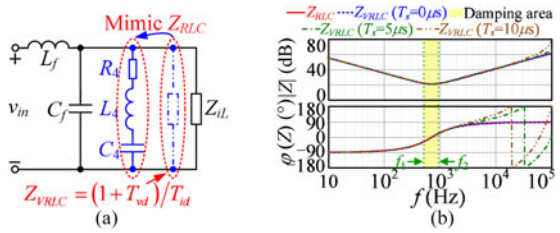


Fig. 8. Comparison of the $RLC$ and $VRLC$ dampers. (a) Function comparison. (b) Bode plots of $Z_{RLC}(s)$ and $Z_{VRLC}(s)$.

By Fig. 7(b), the $VRLC$ damper actually only adds $G_{RLC}(s)$ to the original control system of the CPL. Hence, how to realize $G_{RLC}(s)$ is the key of realizing the $VRLC$ damper. Since Backward Euler, Forward Euler and Tustin are three typical discretization methods in digital control, they are all utilized to convert $G_{RLC}(s)$ to $G_{RLC}(z)$. In order to compare their discretization effect clearly, the Bode plots of $G_{RLC}(s)$ and $G_{RLC}(z)$ with different discretization methods of a specific CPL are depicted in Fig. 7(c), where the example CPL is corresponding to the experimental system in Section V. According to Fig. 7(c), $G_{RLC}(z)$ with the Tustin discretization method is closest one to $G_{RLC}(s)$. Therefore, the Tustin discretization method is selected to convert $G_{RLC}(s)$ to $G_{RLC}(z)$ in the final digital control system of this letter.

### B. Effectiveness Evaluation of the $VRLC$ Damper

Since the purpose of the $VRLC$ damper is to mimic the $RLC$ damper via changing the control block of the $CPL$, the effectiveness of the $VRLC$ damper is evaluated carefully with the comparison of the $RLC$ damper in this section.

According to Fig. 7(b), the input impedance of the CPL with the $VRLC$ damper $Z_{iL}^V(s)$ can be derived as

$$Z_{iL}^V(s) = \left(1/Z_{iL}(s) + 1/Z_{VRLC}(s)\right)^{-1} \tag{18}$$

$$\frac{1}{Z_{iL}(s)} = \frac{1}{Z_{iOL}(s)} \frac{1}{1+T_{\rm vd}(s)} - \frac{T_{\rm vd}(s)}{1+T_{\rm vd}(s)} \frac{P_o}{V_{\rm bus}^2} \tag{19}$$

$$Z_{VRLC}(s) = \left(1+T_{\rm vd}(s)\right)/T_{id}(s) \tag{20}$$

where $T_{\rm vd}(s) = (1/T_s)e^{-sT_s}G_h(s)H_s(s)G_c(s)G_M(s)G_{\rm vd}(s)$ and $T_{id}(s) = (1/T_s)e^{-sT_s}G_h(s)G_{RLC}(s)G_{id}(s)G_M(s)G_c(s)$.

By (18), the $VRLC$ damper adds a virtual impedance $Z_{VRLC}(s)$ in parallel with $Z_{iL}(s)$ to mimic $Z_{RLC}(s)$ as shown in Fig. 8(a). Thus, if the effectiveness of the $VRLC$ damper is required to be evaluated, only one question need to be answered: whether $Z_{VRLC}(s)$ is equal to $Z_{RLC}(s)$ or not? Thus, (17) is substituted into (20) and $Z_{VRLC}(s)$ is

$$Z_{VRLC}(s) \approx Z_{RLC}(s)\left(\frac{e^{1.5sT_s}+T_v(s)}{1+T_v(s)}\right). \tag{21}$$

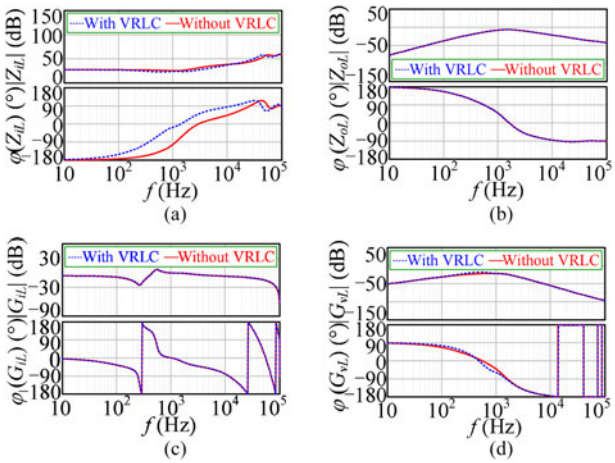


Fig. 9. Impact of the $VRLC$ damper on the CPL: (a) $Z_{iL}(s)$; (b) $Z_{oL}(s)$; (c) $G_{iL}(s)$ and (d) $G_{vL}(s)$.

By (21), if $T_s = 0$, $Z_{VRLC}(s)$ is equal to $Z_{RLC}(s)$; if $T_s \neq 0$, $Z_{RLC}(s)$ and $Z_{VRLC}(s)$ will have difference near the sampling frequency, and the larger $T_s$, the bigger difference. In order to compare $Z_{RLC}(s)$ and $Z_{VRLC}(s)$ clearly, the Bode plots of $Z_{RLC}(s)$ and $Z_{VRLC}(s)$ of a specific CPL are further depicted in Fig. 8(b), where the example CPL is corresponding to the experimental system in Section V. As seen, the curves of $Z_{RLC}(s)$ and $Z_{VRLC}(s)$ are indeed completely coincident when $T_s = 0$. And if $T_s \neq 0$, $Z_{RLC}(s)$ and $Z_{VRLC}(s)$ only become different near sampling frequency and their difference is bigger with the increase of $T_s$. The Bode plots in Fig. 8(b) prove the correctness of (21). Therefore, the effectiveness of the $VRLC$ damper is only affected by the time delay of the digital control system and the smaller time delay the better. In this letter, $T_s$ is selected as $10\,\mu$s. As shown in Fig. 8(b), when $T_s = 10\,\mu$s, $Z_{VRLC}(s)$ mimics $Z_{RLC}(s)$ very well.

Besides, in order to compare the impact of the $RLC$ and $VRLC$ dampers on the $LC$ input filter, the Bode plots of $Z_{\rm ox}(s) \sim G_{\rm ix}(s)$ of the $LC$ input filter with both $RLC$ and $VRLC$ dampers are also depicted in Fig. 3. It is shown that, both $RLC$ and $VRLC$ dampers can improve the performance of the $LC$ input filter and their impact are almost the same. By Fig. 3, it also clearly shows that both $RLC$ and $VRLC$ dampers have better impact than the existing dampers on the $LC$ input filter. Both $RLC$ and $VRLC$ dampers are referred to as "proposed damper" and their impact on the $LC$ input filter are also recorded as "proposed damper" in Table III.

### C. Impact of the $VRLC$ Damper on the CPL

As well known, the performance of the CPL can be fully evaluated by two-port network with four transfer functions [10]: the closed-loop input impedance $Z_{iL}(s)$, the closed-loop output impedance $Z_{oL}(s)$, the closed-loop load to input current transfer function $G_{iL}(s)$, and the closed-loop input to output voltage transfer function $G_{vL}(s)$. Therefore, to evaluate the impact of the $VRLC$ damper on the CPL clearly, the Bode plots of $Z_{iL}(s) \sim Z_{oL}(s)$ of a specific CPL with / without the $VRLC$ damper are depicted in Fig. 9. Here, the example CPL is corresponding to the experimental system in Section V. As seen, apart from adding $Z_{VRLC}(s)$ in parallel with $Z_{iL}(s)$ to mimic the function of the $Z_{RLC}(s)$, the $VRLC$ damper keeps most of the other performances of the original CPL. Thus, the $VRLC$ damper is acceptable in practice.

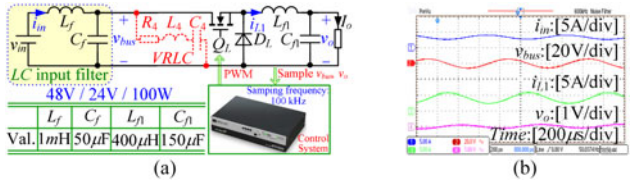


Fig. 10. Experimental system. (a) Main circuit. (b) Steady-state experimental waveforms at rated conditions without any dampers.

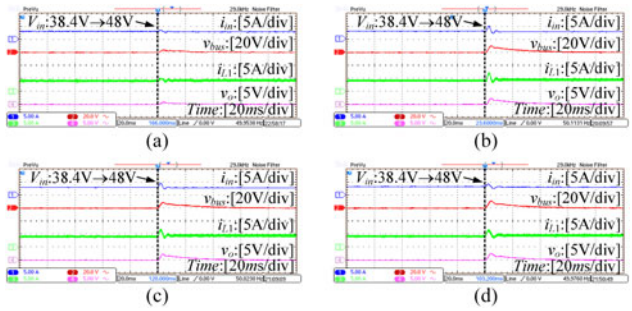


Fig. 11. Experimental waveforms with different dampers when system input voltage changed from 80% to 100% rated voltage at full load: (a) with $VRLC$ damper; (b) with $RC$ parallel damper; (c) with $RL$ parallel damper; (d) with $RL$ series damper.

## V. Experimental Verification

In this letter, experimental results from a 100-W cascaded system are shown to validate the $VRLC$ damper. The main circuit and parameters of the cascaded system are presented in Fig. 10(a), where the parameters of the $VRLC$ damper are: $R_4 = 11.5\,\Omega$, $L_4 = 1.9\,$mH, and $C_4 = 27\,\mu$F. If there is no damper utilized to this system, this system is unstable as shown in Fig. 10(b).

In Fig. 11, the full load experimental results of the cascaded system with different dampers when the input voltage changing from 38.4 to 48 V are given, where $i_{\rm in}$, $v_{\rm bus}$, $i_{L1}$, and $v_o$ are defined in Fig. 10. As seen, both the existing dampers and the $VRLC$ damper can stabilize the unstable cascaded system and make it work well during input voltage changing. Besides, compared to the existing dampers, a better dynamic performance of the $LC$ input filter is gotten by the $VRLC$ damper. The dynamic indicators of the $LC$ input filter with different dampers are also presented in Fig. 12, where, $\sigma_{I_{\rm in}}$ and $t_{I_{\rm in}}$ are the overshoot and regulation time of $i_{\rm in}$, respectively; $\sigma_{V_{\rm bus}}$ and $t_{V_{\rm bus}}$ are the overshoot and regulation time of $v_{\rm bus}$, respectively. As seen, the dynamic indicators of the $LC$ input filter with $VRLC$ damper is indeed better than that with the existing dampers.

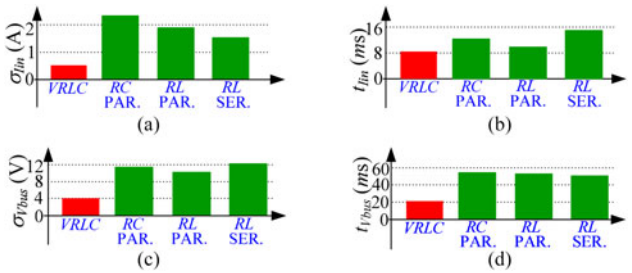


Fig. 12. Comparison of $\sigma_{I_{\rm in}}$, $t_{I_{\rm in}}$, $\sigma_{V_{\rm bus}}$, and $t_{V_{\rm bus}}$ with different dampers when system input voltage changed from 80% to 100% rated voltage at full load: (a) $\sigma_{I_{\rm in}}$; (b) $t_{I_{\rm in}}$; (c) $\sigma_{V_{\rm bus}}$; (d) $t_{V_{\rm bus}}$.

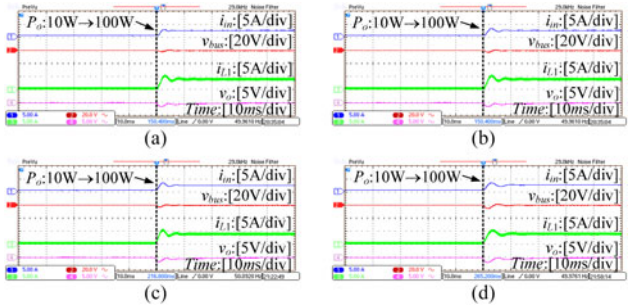


Fig. 13. Experimental waveforms with different dampers when system output power changed from 10 to 100 W at rated input voltage: (a) With $VRLC$ damper; (b) With $RC$ parallel damper; (c) With $RL$ parallel damper; (d) With $RL$ series damper.

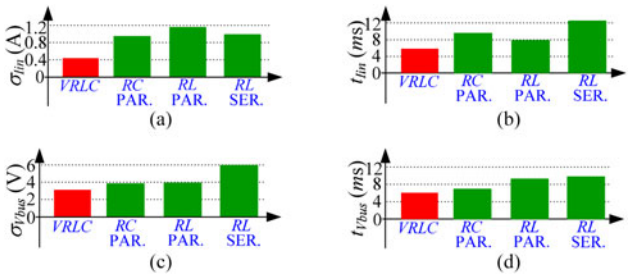


Fig. 14. Comparison of $\sigma_{I_{\rm in}}$, $t_{I_{\rm in}}$, $\sigma_{V_{\rm bus}}$, and $t_{V_{\rm bus}}$ with different dampers when system output power changed from 10 to 100 W at rated input voltage: (a) $\sigma_{I_{\rm in}}$; (b) $t_{I_{\rm in}}$; (c) $\sigma_{V_{\rm bus}}$; (d) $t_{V_{\rm bus}}$.

Similarly, when the output power is changed from 10 to 100 W under rated input voltage, the experimental results of the cascaded system and the dynamic indicators of the $LC$ input filter with different dampers are given in Figs. 13 and 14, respectively. Again, it is verified that, when the load is changing, the $VRLC$ damper still has a better dynamic impact on the $LC$ input filter than the existing dampers.

The efficiency curves of the experimental system with different dampers versus output power and input voltage are measured and plotted in Fig. 15(a) and (b), respectively. As seen, with the $VRLC$ damper, the system efficiency is obviously improved. Therefore, the $VRLC$ damper can stabilize the cascaded system with better performance of the $LC$ input filter and higher efficiency compared with the existing dampers.

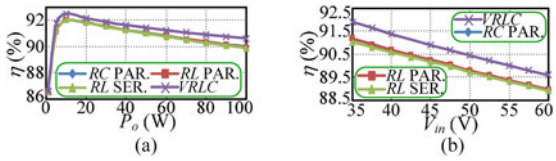


Fig. 15. System efficiency curves with different dampers. (a) Efficiency versus $p_o$ at rated $v_{\rm in}$. (b) Efficiency versus $v_{\rm in}$ at rated $p_o$.

## VI. Conclusion

The impact of the existing dampers on the $LC$ input filter has been first analyzed by the two-port network model in this letter. It is found that, though the existing dampers can solve the instability problem of the CPL with its $LC$ input filter, they degrade the performance of the original $LC$ input filter to some extent. To overcome this drawback, an $RLC$ damper has been proposed in this letter. This damper not only can stabilize the system with improving the input filter performance, but also is robust against the parameter variations of the input filter. To avoid the power loss caused by passive components, the proposed $RLC$ damper is further virtual implemented by control. It is proved that, this $VRLC$ damper not only has the same effectiveness with the $RLC$ damper, but also improves the efficiency of the whole system compared with the existing dampers. Finally, the $VRLC$ damper has been experimentally verified on a 100-W cascaded system.

## Acknowledgment

The authors would like to thank the reviewers for their insightful and interesting comments, which have helped the authors significantly improve the quality of this letter.

## References

[1] Q.-C. Zhong and T. Hornik, *Control of Power Inverters in Renewable Energy and Smart Grid Integration*. New York, NY, USA: Wiley-IEEE, 2013.

[2] R. D. Middlebrook, "Input filter considerations in design and application of switching regulators," in *Proc. IEEE Ind. Appl. Soc.*, May 1979, pp. 366–382.

[3] X. Zhang, X. Ruan, and C. Tse, "Impedance-based local stability criterion for dc distributed power systems," *IEEE Trans. Circuits Syst. I, Reg. Papers*, vol. 62, no. 3, pp. 916–925, Mar. 2015.

[4] R. W. Erickson and D. Maksimov, *Fundamentals of Power Electronics*. Norwell, MA, USA: Kluwer, 2001.

[5] M. Cespedes, L. Xing, and J. Sun, "Constant-power load system stabilization by passive damping," *IEEE Trans. Power Electron.*, vol. 26, no. 7, pp. 1832–1836, Jul. 2011.

[6] D. Marx, P. Magne, B. Nahid-Mobarakeh, S. Pierfederici, and B. Davat, "Large signal stability analysis tools in dc power systems with constant power loads and variable power loads: A review," *IEEE Trans. Power Electron.*, vol. 27, no. 4, pp. 1773–1787, Apr. 2012.

[7] X. Zhang, Q.-C. Zhong, and W. Ming, "Stabilization of a cascaded dc converter system via adding a virtual adaptive parallel impedance to the input of the load converter," *IEEE Trans. Power Electron.*, vol. 31, no. 3, pp. 1826–1832, Mar. 2016.

[8] C. M. Wildrick, "Stability of distributed power supply system," Ph.D. dissertation, Virginia Polytech. Inst. and State Univ., Blacksburg, VA, USA, Feb. 1993.

[9] D. Holmes, T. Lipo, B. McGrath, and W. Kong, "Optimized design of stationary frame three phase ac current regulators," *IEEE Trans. Power Electron.*, vol. 24, no. 11, pp. 2417–2426, Nov. 2009.

[10] X. Zhang, Q.-C. Zhong, and W. Ming, "Stabilization of cascaded dc/dc converters via adaptive series-virtual-impedance control of the load converter," *IEEE Trans. Power Electron.*, vol. 31, no. 9, pp. 6057–6063, Sep. 2016.